

Electromagnetic Signatures of Kinetic Alfvén Wave Turbulence at Ion Inertial Scales in Earth's High- β Magnetosheath

Mani K Chettri^{a,1}, Rupak Mukherjee^a and Hemam D. Singh^{b,*}

^aDepartment of Physics, Sikkim University, Gangtok, 737102, Sikkim, India

^bDepartment of Physics, Netaji Subhas University of Technology, New Delhi, 110078, India

ARTICLE INFO

Keywords:

Magnetosheath
Kinetic Alfvén waves
MMS observations
Ion inertial scale
Magnetic compressibility
Wave-particle interactions

ABSTRACT

We present a multi-diagnostic electromagnetic study of kinetic Alfvén wave (KAW) activity in Earth's magnetosheath using burst-mode measurements from the Magnetospheric Multiscale (MMS) mission. We apply this analysis to a well-characterized dayside magnetosheath interval on 2015 December 28 at unusually high plasma $\beta_i \approx 14$. The identification relies on four simultaneous criteria: the normalized electric-to-magnetic field ratio $\delta E_{\perp}/(\delta B_{\perp} v_A)$ exceeding the ideal MHD limit (median 2.55), the presence of a finite parallel electric field δE_{\parallel} (peak 3.2 mV m^{-1}), a spectral break at the ion inertial scale $k_{\perp} d_i \approx 1$ (where $d_i = 45.0 \text{ km}$ is the ion inertial length, the theoretically expected transition scale at $\beta_i \gg 1$), and a kinetic-range magnetic compressibility $C_B = 0.31$ within the KAW-predicted range [0.10, 0.40]. All four criteria are satisfied in the same interval, providing a consistent electromagnetic identification of KAWs that does not require particle distribution measurements. A key result of this analysis is the clear identification of d_i rather than the ion gyroradius $\rho_i = 170.4 \text{ km}$ as the relevant spectral break scale. At $\beta_i = 14.4$, the two scales differ by a factor of 3.79, making this distinction observationally testable in a way that is not possible at the more typical magnetosheath $\beta \sim 1-5$. The spectral break at $f_{\text{break}} \approx 0.6 \text{ Hz}$ is consistent with $k_{\perp} d_i \approx 1$ given the measured bulk flow $V_{\text{flow}} = 159 \text{ km s}^{-1}$, but inconsistent with $k_{\perp} \rho_i \approx 1$, which would require $V_{\text{flow}} \approx 640 \text{ km s}^{-1}$. Magnetic power spectral analysis reveals an inertial-range scaling of $f^{-1.84}$, steepened relative to Kolmogorov by the compressible, shock-processed character of the magnetosheath, and a kinetic-range slope of $f^{-3.31}$ above the spectral break. This kinetic-range index lies between the theoretical predictions for an undamped dispersive KAW cascade ($-8/3$) and a cascade strongly suppressed by Landau damping ($-11/3$), consistent with an intermediate dissipation state.

1. Introduction

Earth's magnetosheath, the turbulent compressed plasma occupying the region immediately downstream of the bow shock, provides an accessible high- β laboratory for studying kinetic-scale plasma turbulence and energy dissipation. Unlike the ambient solar wind, where $\beta \sim 1$ is typical, the magnetosheath regularly sustains $\beta \sim 1-10$ (Lucek, Constantinescu, Goldstein, Pickett, Pinçon, Sahraoui, Treumann and Walker, 2005; Alexandrova, Lacombe and Mangeney, 2008; Macek, Krasnińska, Silveira, Sibek, Wawrzaszek, Burch and Russell, 2018; Sahraoui, Hadid and Huang, 2020), placing it in a regime where the dispersive and dissipative properties of kinetic Alfvén waves (KAWs) are strongly β -dependent and wave-particle resonances are particularly efficient.

KAWs constitute the dispersive continuation of the shear Alfvén mode at perpendicular scales $k_{\perp} \rho_i \gtrsim 1$, where ρ_i is the ion thermal gyroradius. Two electromagnetic signatures distinguish them from ideal magnetohydrodynamic (MHD) Alfvén waves: a nonzero parallel electric field δE_{\parallel} , which drives field-aligned electron acceleration, and an enhanced ratio of perpendicular electric to magnetic field fluctuations $\delta E_{\perp}/(\delta B_{\perp} v_A) > 1$ (Hasegawa, 1976; Hollweg, 1999; Stasiewicz, Bellan, Chaston, Kletzing, Lysak, Maggs, Pokhotelov, Seyler, Shukla, Stenflo, Streltsov and Wahlund, 2000). The parallel electric field is particularly important because it enables Landau resonance with electrons satisfying $v_{\parallel} \approx \omega/k_{\parallel}$, establishing KAWs as primary vectors of turbulent energy dissipation in collisionless high- β plasmas (Howes, 2015; Chen, Klein and Howes, 2019; Afshari, Howes, Kletzing, Hartley and Boardsen, 2021; Schekochihin, Cowley, Dorland, Hammett, Howes, Quataert and Tatsuno, 2009).

*Corresponding author

✉ hemam.singh@nsut.ac.in (H. D. Singh)

ORCID(s): 0009-0000-1368-9263 (M.K. Chettri); 0000-0003-3955-7116 (R. Mukherjee); 0009-0003-3061-8944 (H. D. Singh)

¹Electronic email: mkchettri8@gmail.com

The Magnetospheric Multiscale (MMS) mission, with its burst-mode sampling of 128 Hz for magnetic fields and concurrent electric field and particle measurements, has substantially advanced observational access to these kinetic-scale processes (Burch, Moore, Torbert and Giles, 2016; Russell, Anderson, Baumjohann, Bromund, Dearborn, Fischer, Le, Leinweber, Leneman, Magnes, Means, Moldwin, Nakamura, Pierce, Plaschke, Rowe, Slavin, Strangeway, Torbert, Hagen, Jernej, Valavanoglou and Richter, 2016; Pollock, Moore, Jacques, Burch, Gliese, Saito, Omoto, Avakov, Barrie, Coffey, Dorelli, Gershman, Giles, Rosnack, Salo, Yokota, Adrian, Aoustin, Aulletti, Aung, Bigio, Cao, Chandler, Chornay, Christian, Clark, Collinson, Corris, De Los Santos, Devlin, Diaz, Dickerson, Dickson, Diekmann, Diggs, Duncan, Figueroa-Vinas, Firman, Freeman, Galassi, Garcia, Goodhart, Guererro, Hageman, Hanley, Hemminger, Holland, Hutchins, James, Jones, Kreisler, Kujawski, Lavu, Lobell, LeCompte, Lukemire, MacDonald, Mariano, Mukai, Narayanan, Nguyen, Onizuka, Paterson, Persyn, Piepgrass, Cheney, Rager, Raghuram, Ramil, Reichenthal, Rodriguez, Rouzard, Rucker, Saito, Samara, Sauvaud, Schuster, Shappirio, Shelton, Sher, Smith, Smith, Smith, Steinfeld, Szymkiewicz, Tanimoto, Taylor, Tucker, Tull, Uhl, Vloet, Walpole, Weidner, White, Winkert, Yeh and Zeuch, 2016). Studies using MMS have reported individual KAW wave packets in magnetosheath reconnection regions (Gershman, F-Viñas, Dorelli, Boardsen, Avakov, Bellan, Schwartz, Lavraud, Coffey, Chandler, Saito, Paterson, Fuselier, Ergun, Strangeway, Russell, Giles, Pollock, Torbert and Burch, 2017; Stawarz, Eastwood, Phan, Gingell, Pyakurel, Shay, Robertson, Russell and Le Contel, 2022), field-particle correlation evidence of Landau damping (Afshari et al., 2021), and systematic spectral steepening near the ion gyrofrequency (Macek et al., 2018; Macek and Wójcik, 2023). KAW turbulence and nonlinear wave coupling have similarly been reported in the inner heliosphere and the plasma sheet boundary layer (Chettri, Shrivastav, Mukherjee, Gaur, Sharma and Singh, 2024; Chettri, Singh and Mukherjee, 2026), motivating the multi-diagnostic approach applied here.

Prior spectral analyses of the 2015 December 28 MMS magnetosheath interval by Macek et al. (2018) and Macek and Wójcik (2023) established the two-range spectral structure and documented ion-scale steepening at conditions of $\beta \sim 2-5$. The present study extends that work in three respects. First, we analyze this interval at the event-specific ion beta $\beta_i = 14.4$, which places it at the high- β end of magnetosheath conditions and allows the ion inertial length d_i and the ion gyroradius ρ_i to be distinguished observationally: the two scales differ here by a factor of 3.79, and we show that the spectral break locates at d_i , not ρ_i , consistently with theoretical expectations for $\beta_i \gg 1$ (Hasegawa, 1976; Stasiewicz et al., 2000). This distinction is not testable at $\beta \sim 1-5$ where the two scales differ by at most a factor of two. Second, we apply four independent electromagnetic diagnostics simultaneously to the same observational interval, including the E/B ratio normalized to the Alfvén speed v_A , the parallel electric field, the spectral break scale, and the magnetic compressibility C_B , providing a multi-layered mode identification that does not rest on any single criterion and rules out the main alternative interpretations (mirror modes, whistlers) from electromagnetic data alone. Third, we place the kinetic-range spectral index within the theoretical framework of Boldyrev and Perez (2012) and Passot and Sulem (2015) to obtain a direct observational constraint on the effective dissipation level, and discuss how this approach could be extended to statistical surveys using standard burst-mode magnetometer data.

2. Data and Interval Selection

We analyze MMS1 Level-2 burst-mode data from 2015 December 28, 01:48:00–01:52:30 UT, during which the spacecraft was positioned in the dayside magnetosheath at $(X, Y, Z)_{\text{GSE}} = (10.2, -5.8, -1.0) R_E$. This interval was identified in prior MMS analyses as exhibiting a well-defined two-range magnetic power spectrum with steepening near ion scales and pronounced Alfvénic fluctuations (Macek et al., 2018; Macek and Wójcik, 2023), confirming its suitability as a testbed for kinetic-scale electromagnetic analysis. Those studies focused on the magnetic field spectrum; the plasma β environment for this specific event was not their primary reported quantity.

The present study independently characterizes the plasma environment using burst-mode FPI moments computed directly over the 4.5-minute window, yielding $\beta_i = 14.4$ (Table 1). Fast-survey FPI data over the full 70-minute magnetosheath pass confirm that β_i remains elevated ($\beta_i \sim 10-40$) throughout, with a median of ≈ 14.8 during the burst interval, establishing that the analyzed data represent a stable, typical high- β magnetosheath environment rather than an isolated transient excursion. Direct computation from the burst-mode plasma and field measurements yields a high- β environment: $\beta_i = 14.4$, $\beta_e = 1.6$, $\beta_{\text{tot}} = 16.0$ (see Table 1).

Three MMS instrument suites are used. The FluxGate Magnetometer (FGM) provides vector magnetic field measurements at 128 Hz (Russell et al., 2016). The Electric Double Probe (EDP) provides three-component electric field measurements at comparable cadence (Torbert, Russell, Magnes, Ergun, Lindqvist, LeContel, Vaith, Macri, Myers, Rau, Needell, King, Granoff, Chutter, Dors, Olsson, Khotyaintsev, Eriksson, Kletzing, Bounds, Anderson,

Baumjohann, Steller, Bromund, Le, Nakamura, Strangeway, Leinweber, Tucker, Westfall, Fischer, Plaschke, Porter and Lappalainen, 2016). The Fast Plasma Investigation (FPI) provides ion and electron moments at 150 ms and 30 ms cadence respectively, which we use for background plasma characterization (Pollock et al., 2016). Data are retrieved and processed using the PySPEDAS library (Angelopoulos, Cruce, Drozdov, Grimes, Hatzigeorgiu, King, Larson, Lewis, McTiernan, Roberts, Russell, Hori, Kasahara, Kumamoto, Matsuoka, Miyashita, Miyoshi, Shinohara, Teramoto, Faden, Halford, McCarthy, Millan, Sample, Smith, Woodger, Masson, Narock, Asamura, Chang, Chiang, Kazama, Keika, Matsuda, Segawa, Seki, Shoji, Tam, Umemura, Wang, Wang, Redmon, Rodriguez, Singer, Vandegriff, Abe, Nose, Shinbori, Tanaka, UeNo, Andersson, Dunn, Fowler, Halekas, Hara, Harada, Lee, Lillis, Mitchell, Argall, Bromund, Burch, Cohen, Galloy, Giles, Jaynes, Le Contel, Oka, Phan, Walsh, Westlake, Wilder, Bale, Livi, Pulupa, Whittlesey, DeWolfe, Harter, Lucas, Auster, Bonnell, Cully, Donovan, Ergun, Frey, Jackel, Keiling, Korth, McFadden, Nishimura, Plaschke, Robert, Turner, Weygand, Candey, Johnson, Kovalick, Liu, McGuire, Breneman, Kersten and Schroeder, 2019; Grimes, Harter, Hatzigeorgiu, Drozdov, Lewis, Angelopoulos, Cao, Chu, Hori, Matsuda, Jun, Nakamura, Kitahara, Segawa, Miyoshi and Le Contel, 2022), including standard spike removal, coordinate transformation to Geocentric Solar Ecliptic (GSE) coordinates, and linear detrending prior to spectral analysis. For wave analysis, a background field is estimated with a 10 s sliding window (corresponding to the lower cutoff of the [0.1, 2.0] Hz bandpass) and subtracted; electric and magnetic fluctuations are then decomposed into field-aligned (parallel) and perpendicular components. Throughout this paper, ‘parallel’ and ‘perpendicular’ refer to directions relative to the background magnetic field \mathbf{B}_0 . A bandpass filter of [0.1, 2.0] Hz isolates fluctuations in the transition from inertial to kinetic scales. Power spectral densities are computed using Welch’s method (Welch, 1967) with a Hanning window ($N_{\text{seg}} = 2048$ points, 50% overlap) applied to the B_L component in local LMN coordinates, yielding a frequency resolution of 0.0625 Hz.

The time-averaged plasma parameters computed directly from the burst-mode data are listed in Table 1. The background magnetic field is $B_0 = 17.8 \pm 8.2$ nT, the ion density $n_i = 25.6 \pm 7.6$ cm⁻³, and the ion (electron) temperature $T_i = 0.44$ keV ($T_e = 0.047$ keV), giving an ion beta $\beta_i = 14.4$. The Alfvén speed is $v_A = 77$ km s⁻¹, and the ion inertial length $d_i = 45.0$ km. The ion thermal gyroradius is $\rho_i = 170.4$ km, with $\rho_i/d_i = \sqrt{\beta_i} = 3.79$ as expected. The bulk plasma flow velocity $V_{\text{flow}} = 159 \pm 33$ km s⁻¹, giving $V_{\text{flow}}/v_A = 2.1$; this satisfies the Taylor frozen-in criterion $V_{\text{flow}} > v_A$ marginally, and we assess its implications in Section 4.1.

3. Multi-Diagnostic KAW Identification

Figure 1, panel (a) of which is adapted from Chettri, Singh, Shrivastav, Singh and Mukherjee (2025), presents the four-panel electromagnetic analysis. Panel (a) shows the amplitude of perpendicular electric field fluctuations δE_{\perp} , which range up to ~ 4.5 mV m⁻¹. Panel (b) shows perpendicular magnetic field fluctuations δB_{\perp} (RMS 5.22 nT), spanning up to ~ 27 nT. Both time series are correlated and display a distinctly intermittent, bursty character rather than a smooth continuous oscillation, consistent with the spatial inhomogeneity of turbulence in the shocked magnetosheath (Roberts, Toledo-Redondo, Perrone, Zhao, Narita, Gershman, Nakamura, Lavraud, Escoubet, Giles, Dorelli, Pollock and Burch, 2018).

Panel (c) shows the parallel electric field amplitude δE_{\parallel} , which reaches up to 3.2 mV m⁻¹. This quantity is the most direct electromagnetic discriminator between KAWs and ideal MHD Alfvén waves: MHD strictly requires $\delta E_{\parallel} = 0$, while KAWs generically support finite δE_{\parallel} through the combined effects of electron inertia and electron thermal pressure gradients along the field (Lysak and Lotko, 1996; Wygant, Keiling, Cattell, Lysak, Temerin, Mozer, Kletzing, Scudder, Streltsov, Lotko and Russell, 2002; Ergun, Tucker, Westfall, Goodrich, Malaspina, Summers, Wallace, Karlsson, Mack, Brennan, Pyke, Withnell, Torbert, Macri, Rau, Dors, Needell, Lindqvist, Olsson and Cully, 2016). The observed peak $\delta E_{\parallel} = 3.2$ mV m⁻¹ is comparable to the RMS $\delta E_{\perp} = 1.08$ mV m⁻¹, confirming a substantial parallel component and supporting the kinetic nature of the fluctuations. We note that the EDP axial component (E_z in spacecraft coordinates) is reconstructed under the assumption $\mathbf{E} \cdot \mathbf{B} = 0$ at low frequencies, and this reconstruction becomes less reliable at frequencies approaching f_{ci} . The δE_{\parallel} magnitudes in Figure 1(c) should therefore be interpreted with this caveat in mind, although the qualitative hierarchy $\delta E_{\parallel} \sim \delta E_{\perp} \gg 0$ is robust to this uncertainty.

Panel (d) shows the normalized ratio $\delta E_{\perp}/(\delta B_{\perp} v_A)$. For ideal MHD Alfvén waves this quantity equals unity; for KAWs it exceeds unity by an amount that increases with $k_{\perp} \rho_i$ and depends on plasma β (Stasiewicz et al., 2000; Salem, Howes, Sundkvist, Bale, Chaston, Chen and Mozer, 2012; Bale, Kellogg, Mozer, Horbury and Rème, 2005). The observed ratio has a median of 2.55 (IQR: 1.43–5.00), consistently exceeding the MHD limit (black dashed line) throughout the interval and frequently falling within the KAW-expected range (green shaded region).

Table 1

Plasma parameters for MMS-1, 2015 December 28, 01:48:00–01:52:30 UTC (dayside magnetosheath). Ion scalar temperature $T_i = (T_{i\parallel} + 2T_{i\perp})/3$ is used for β_i ; perpendicular temperature $T_{i\perp}$ is used for ρ_i . Wave amplitudes use a [0.1, 2.0] Hz bandpass. The normalized $\delta E/\delta B$ ratio is reported as median with interquartile range (IQR).

Parameter	Symbol	Value	Unit
<i>Observational parameters</i>			
SC position (GSE)	(X, Y, Z)	(10.2, -5.8 , -1.0)	R_E
Background magnetic field	B_0	17.8 ± 8.2	nT
Ion number density	n_i	25.6 ± 7.6	cm^{-3}
Ion temperature (scalar)	T_i	0.442 ± 0.120	keV
Ion temperature (perp)	$T_{i\perp}$	0.440 ± 0.120	keV
Electron temperature	T_e	0.047 ± 0.004	keV
Temperature ratio	T_i/T_e	9.3	–
Ion beta	β_i	14.4	–
Electron beta	β_e	1.6	–
Total beta	β_{tot}	16.0	–
Bulk flow speed	V_{flow}	159 ± 33	km s^{-1}
<i>Derived characteristic scales</i>			
Alfvén speed	v_A	77	km s^{-1}
Ion gyroradius (\perp)	ρ_i	170.4	km
Ion inertial length	d_i	45.0	km
Ion length ratio	ρ_i/d_i	$3.79 (= \sqrt{\beta_i})$	–
Ion cyclotron frequency	f_{ci}	0.271	Hz
<i>Wave properties (bandpass [0.1, 2.0] Hz)</i>			
RMS electric field	$\langle \delta E_{\perp}^2 \rangle^{1/2}$	1.08	mV m^{-1}
RMS magnetic field	$\langle \delta B_{\perp}^2 \rangle^{1/2}$	5.22	nT
Peak parallel field	$E_{\parallel, \text{max}}$	3.2	mV m^{-1}
Norm. $\delta E/\delta B$ (median)	$\delta E_{\perp}/(v_A \delta B_{\perp})$	2.55 [IQR: 1.43–5.00]	–

The physical significance of these observations is sharpened by the temporal coincidence of all four electromagnetic signatures. Two particularly well-defined episodes near 01:50:00 and 01:51:00 UT show simultaneous enhancement in $\delta E_{\perp}/(\delta B_{\perp} v_A)$, elevated δE_{\parallel} , and organized magnetic fluctuation structure. These localized bursts are consistent with coherent KAW wave packets embedded in the broader turbulent background, analogous to those reported by Gershman et al. (2017) and Roberts et al. (2018) in the magnetosheath. The coincidence of all four independent criteria in the same interval is the key discriminator: individual criteria can, in principle, be satisfied by other wave modes such as mirror modes or whistlers, but their simultaneous occurrence with the correct amplitude ordering constitutes a robust electromagnetic fingerprint of KAWs that does not require particle distribution function measurements.

4. Spectral Analysis and Dissipation Constraint

Figure 2 shows the magnetic power spectral density (PSD) computed from the burst-mode FGM data over the full 4.5-minute interval.

4.1. Two-range spectral structure

The spectrum shows a well-defined two-range structure separated by a spectral break near $f_{\text{break}} \approx 0.6$ Hz. In the inertial range ($0.05 < f < 0.6$ Hz), the PSD follows a power law with index -1.84 . This is noticeably steeper than the standard incompressible Kolmogorov slope of $-5/3$, but is a well-documented characteristic of magnetosheath turbulence. The enhanced compressibility of post-shock plasma, the presence of intermittent structures and shocklets, and the more symmetric distribution of Alfvénic propagation directions compared to the solar wind all act to modify the energy transfer rate and steepen the inertial-range spectrum (Hadid, Sahraoui and Galtier, 2017; Hadid, Sahraoui, Galtier and Huang, 2018; Macek et al., 2018). This steepening is a fluid-scale effect and is distinct from the kinetic dissipation processes that operate above f_{break} .

Above the spectral break, in the kinetic range ($f > 3$ Hz), the spectrum steepens further to $f^{-3.31}$. We interpret this break as the transition from fluid to kinetic dynamics at the ion inertial scale $k_{\perp}d_i \approx 1$. In this high- β interval ($\beta_i = 14.4$), the ion inertial length $d_i = 45.0$ km rather than the ion gyroradius $\rho_i = 170.4$ km is the relevant transition scale, because at $\beta_i \gg 1$ the dispersive modification to Alfvén waves occurs at $k_{\perp}d_i \sim 1$ (Hasegawa, 1976; Leamon, Smith, Ness, Matthaeus and Wong, 1998). To evaluate this, we apply Taylor's frozen-in hypothesis (Taylor, 1938), which relates the spacecraft-frame frequency f to the plasma-frame perpendicular wavenumber via $k_{\perp} = 2\pi f/V_{\text{flow}}$. The condition $k_{\perp}d_i = 1$ at the break frequency gives:

$$V_{\text{flow}} = 2\pi f_{\text{break}} d_i = 2\pi \times 0.6 \times 45.0 \approx 170 \text{ km s}^{-1}, \quad (1)$$

which is consistent with the measured bulk flow velocity $V_{\text{flow}} = 159 \pm 33 \text{ km s}^{-1}$ to within measurement uncertainty. A useful property of the Taylor mapping is that spectral indices are preserved: if $P(k) \propto k^{\alpha}$ in the plasma frame, then $P(f) \propto f^{\alpha}$ in the spacecraft frame, so the observed indices -1.84 and -3.31 translate directly into wavenumber-space slopes for comparison with theory. We note that with $V_{\text{flow}}/v_A = 2.1$, the Taylor frozen-in condition is only marginally satisfied. However, at sub-ion scales ($k_{\perp}d_i > 1$), the perpendicular phase speed of KAWs remains small compared with the bulk flow, so perpendicular sweeping continues to dominate the frequency-to-wavenumber mapping (Howes, Klein and TenBarge, 2014; Klein, Howes and TenBarge, 2014). In this moderate-flow regime, the partial breakdown of Taylor's hypothesis primarily introduces minor frequency broadening rather than a fundamental shift in the location of the spectral break. The $\sim 10\%$ discrepancy between the theoretically predicted and observationally measured flow speeds falls comfortably within this expected broadening, as well as the natural spatial inhomogeneity of the background plasma over the 4.5-minute window. This consistency confirms that $f_{\text{break}} \approx 0.6$ Hz marks the ion inertial scale $k_{\perp}d_i \approx 1$, as expected for high- β kinetic turbulence.

4.2. Kinetic-range index as a dissipation gauge

The kinetic-range spectral index of -3.31 can be placed in context using two theoretical limiting cases established in the literature. In the absence of significant collisionless dissipation, the KAW turbulent cascade is governed by dispersive nonlinear interactions. Theoretical work (Boldyrev and Perez, 2012; Howes, Dorland, Cowley, Hammett, Quataert, Schekochihin and Tatsuno, 2008) and observations (Sahraoui et al., 2009; Sahraoui, Goldstein, Belmont, Canu and Rezeau, 2010) consistently find a kinetic-range spectrum scaling as $k_{\perp}^{-8/3} \approx k_{\perp}^{-2.67}$ in this conservative regime. At the other extreme, when Landau damping strongly suppresses the cascade, the spectrum steepens toward $k_{\perp}^{-11/3} \approx k_{\perp}^{-3.67}$ (Passot and Sulem, 2015; Alexandrova et al., 2012).

The observed index -3.31 falls between these two limits, $-8/3 \approx -2.67 < -3.31 < -3.67 \approx -11/3$. This positioning is physically meaningful. A slope of -2.67 would indicate that the cascade proceeds from ion to electron scales with negligible particle heating; the spectrum is conservative. A slope of -3.67 would indicate that the cascade is so efficiently damped that most energy is deposited in particles before reaching electron scales. This positioning is consistent with a state in which wave-particle interactions are present but neither negligible nor fully dominant over the turbulent cascade. We caution that the spectral index alone cannot distinguish between Landau damping and other collisionless dissipation channels (e.g. stochastic heating, transit-time damping); it constrains the *effective* dissipation level relative to the two theoretical limits, not the specific mechanism. The large $\beta_i = 14.4$ is notable in this context: at $\beta_i \gg 1$ the resonant condition $v_{\parallel} \approx \omega/k_{\parallel} \approx v_A$ lies well within the ion thermal distribution, making wave-particle interactions kinematically accessible to a large fraction of the particle population (Howes, 2015; TenBarge and Howes, 2013).

Afshari et al. (2021) showed that Landau damping signatures are present in 95% of MMS magnetosheath intervals but their amplitude varies considerably. The spectral index provides a single macroscopic observable that encodes this variability in a way that is accessible from magnetic field data alone, without requiring field-particle correlation analysis or distribution function measurements.

The observed spectral properties of this interval are summarized in Table 2.

4.3. Magnetic polarization and compressibility

Figure 3 provides an independent mode identification by decomposing the burst-mode FGM magnetic fluctuations in field-aligned coordinates (FAC) and computing the magnetic compressibility

$$C_B(f) = \frac{P_{B\parallel}}{P_{B\parallel} + P_{B\perp}}, \quad (2)$$

Table 2

Observed magnetic spectral properties, MMS1, 2015 December 28.

Property	Observed value
Inertial-range index	−1.84
Kinetic-range index	−3.31
Spectral break frequency	≈ 0.6 Hz
Corresponding plasma scale	$k_{\perp}d_i \approx 1$
Implied flow velocity	≈ 170 km s ^{−1}
Measured bulk flow	159 ± 33 km s ^{−1}
Plasma β_i	14.4

where $P_{B\parallel}$ and $P_{B\perp}$ are the power spectral densities of field-parallel and field-perpendicular magnetic fluctuations, respectively. The FAC basis is constructed from a 10 s moving average of the measured field, identical to the background subtraction used in Section 2.

Panel (a) of Figure 3 shows $P_{B\perp}(f)$ and $P_{B\parallel}(f)$ separately. In the inertial range the two components carry approximately equal power ($P_{B\perp}/P_{B\parallel} \approx 1.0$), consistent with isotropic large-scale MHD Alfvénic turbulence. Above the ion-scale break at $k_{\perp}d_i = 1$ (0.56 Hz, green line), the perpendicular component dominates: the median ratio $P_{B\perp}/P_{B\parallel} = 2.2$ in the kinetic range indicates predominantly transverse magnetic fluctuations, the expected FAC signature of KAWs whose energy is carried in perpendicular field distortions (Hasegawa, 1976; Stasiewicz et al., 2000). Panel (b) shows the magnetic compressibility $C_B(f)$. The median value in the kinetic range is $C_B = 0.31$, which falls within the theoretical KAW prediction of $C_B \in [0.10, 0.40]$ (Sahraoui et al., 2009; Stasiewicz et al., 2000). This directly excludes the two main alternative interpretations: mirror modes, which are purely compressive ($C_B \sim 0.8\text{--}1.0$), and whistler-mode waves, which also exhibit high compressibility ($C_B \gtrsim 0.5$) at sub-ion scales. The transition from moderately compressive ($C_B \approx 0.4\text{--}0.7$, inertial range) to low-compressibility ($C_B \approx 0.31$, kinetic range) occurs precisely at the $k_{\perp}d_i = 1$ scale identified in the PSD (Figure 2), providing an internally consistent and physically meaningful confirmation of the ion-scale spectral break.

5. Discussion

Robustness of the multi-diagnostic identification: The simultaneous satisfaction of four independent electromagnetic criteria, the E/B ratio (median 2.55, well above unity), finite δE_{\parallel} (peak 3.2 mV m^{−1}), the spectral break at $k_{\perp}d_i \approx 1$, and magnetic compressibility $C_B = 0.31$ within the KAW-predicted range, establishes a redundant and internally consistent identification of KAW-dominated fluctuations. Each diagnostic is mechanistically distinct: the E/B ratio reflects the wave dispersion relation, the parallel electric field reflects electron kinetics along the background field, the spectral break reflects the scale at which ion inertial effects modify the turbulent cascade, and C_B directly measures the compressive versus transverse partitioning of magnetic energy. The C_B measurement is particularly valuable because it independently discriminates against mirror modes and whistler modes that can, in principle, satisfy the E/B or δE_{\parallel} criteria under special circumstances. Their simultaneous occurrence in the same interval, with C_B transitioning from isotropic (≈ 0.5) to the KAW range (≈ 0.31) exactly at the $k_{\perp}d_i = 1$ break, constitutes a self-consistent, multi-layered electromagnetic identification of KAWs. This approach is applicable wherever burst-mode FGM data are available and requires no particle measurements.

Dissipation state and spectral index: The kinetic-range index −3.31 provides an observational constraint on the dissipation state of the cascade. Its deviation from −8/3 is consistent with the cascade being attenuated relative to the purely dispersive case; its separation from −11/3 suggests that a substantial fraction of energy survives to smaller scales. The high $\beta_i = 14.4$ is relevant in this context: at $\beta_i \gg 1$ the ion thermal velocity substantially exceeds v_A , so wave-particle resonance conditions are kinematically accessible to a large fraction of the particle population (Howes, 2015; Chen et al., 2019; Horvath, Howes and McCubbin, 2020). Whether this results in preferential ion or electron energization cannot be determined from electromagnetic data alone, but the $T_i/T_e = 9.3$ temperature ratio is consistent with scenarios in which wave-particle interactions transfer energy preferentially to ions at high β (Afshari et al., 2021; Bandyopadhyay, Matthaeus, Parashar, Yang, Chasapis, Giles, Gershman, Pollock, Russell, Strangeway, Torbert, Moore and Burch, 2020). We note that the spectral index alone does not identify the specific dissipation channel; Landau

damping, stochastic heating, and transit-time damping all produce cascade steepening and cannot be distinguished from this measurement. A useful extension of this approach would be to compile kinetic-range spectral indices from many MMS magnetosheath intervals and correlate them with local β_i and independently measured dissipation proxies such as the field-particle correlation signatures of Afshari et al. (2021), building an empirical calibration between the spectral index and the dissipation level across varying plasma conditions. The spectral index, computed from standard burst-mode FGM data, offers an effective primary diagnostic for such a survey.

Inertial-range steepening: The inertial-range slope -1.84 , steeper than Kolmogorov $-5/3$, should not be attributed to kinetic dissipation. The steepening in the inertial range ($f < 0.6$ Hz) is a well-understood fluid-scale consequence of compressibility, intermittency, and bow-shock imprinting on the downstream plasma (Hadid et al., 2017, 2018; Macek et al., 2018). The spectral break at $f \approx 0.6$ Hz clearly separates the inertial and kinetic dissipation regimes. The two ranges respond to different physics: compressibility modifies the inertial range, while wave-particle dissipation governs the kinetic range. This separation is evident in the spectral structure and should be borne in mind when comparing magnetosheath spectral indices with solar wind or numerical simulation results.

High- β context and kinetic scale identification: The high ion beta $\beta_i = 14.4$ of this interval places it at the upper end of magnetosheath conditions (Lucek et al., 2005; Macek et al., 2018) and has direct consequences for the scale identification. When $\beta_i \gg 1$, the ion inertial length d_i and the ion gyroradius ρ_i are related by $\rho_i = \sqrt{\beta_i} d_i$; here $\rho_i = 3.79 d_i = 170.4$ km versus $d_i = 45.0$ km. The spectral break at $f_{\text{break}} \approx 0.6$ Hz satisfies $k_{\perp} d_i \approx 1$ (consistent with measured V_{flow}) but $k_{\perp} \rho_i \approx 4$ (inconsistent). This unambiguously identifies d_i as the relevant transition scale, consistent with the theoretical expectation that at $\beta \gg 1$, dispersive effects in KAW physics first appear at $k_{\perp} d_i \sim 1$ (Hasegawa, 1976; Stasiewicz et al., 2000). This distinction matters for future surveys: at typical magnetosheath $\beta \sim 1-5$, d_i and ρ_i differ by factors of 1–2 and may both contribute to spectral features; at $\beta \sim 14$, d_i uniquely identifies the break, which is valuable for constraining the underlying wave physics.

Limitations: This analysis is based on a single spacecraft and a single 4.5-minute interval. While the interval is representative of dayside magnetosheath conditions and has been independently validated in prior studies (Macek et al., 2018; Stawarz and Genestreti, 2023), a statistical survey of many MMS magnetosheath intervals at different β values, solar wind conditions, and magnetosheath locations (subsolar, flank) would substantially strengthen the conclusions and allow the spectral dissipation gauge to be calibrated against local plasma parameters. Such an extension is a natural and straightforward application of the methodology developed here.

6. Conclusion

Using MMS1 burst-mode electromagnetic measurements in the dayside magnetosheath on 2015 December 28, we have identified the following key points:

1. Four independent electromagnetic diagnostics, the normalized E/B ratio $\delta E_{\perp}/(\delta B_{\perp} v_A)$ with median 2.55 (well above the MHD limit of unity), finite parallel electric field δE_{\parallel} reaching 3.2 mV m $^{-1}$, a spectral break at the ion inertial scale $k_{\perp} d_i \approx 1$ (consistent with measured $V_{\text{flow}} = 159$ km s $^{-1}$), and magnetic compressibility $C_B = 0.31$ in the kinetic range (within the KAW-predicted range [0.10, 0.40], excluding mirror modes and whistlers), are simultaneously satisfied, providing a consistent multi-diagnostic electromagnetic identification of KAWs without requiring particle distribution measurements.
2. The unusually high $\beta_i = 14.4$ of this interval allows $d_i = 45.0$ km and $\rho_i = 170.4$ km to be distinguished observationally. The spectral break at $f_{\text{break}} \approx 0.6$ Hz is consistent with $k_{\perp} d_i \approx 1$ given the measured flow speed, but inconsistent with $k_{\perp} \rho_i \approx 1$, which would require $V_{\text{flow}} \approx 640$ km s $^{-1}$. This unambiguously identifies d_i as the relevant transition scale, consistent with theoretical expectations for $\beta_i \gg 1$ (Hasegawa, 1976; Stasiewicz et al., 2000).
3. The magnetic power spectrum steepens from $f^{-1.84}$ in the inertial range, where compressibility and bow-shock effects modify the fluid cascade, to $f^{-3.31}$ in the kinetic range above the ion-scale spectral break at $f \approx 0.6$ Hz. The kinetic-range index -3.31 lies between the theoretical predictions for an undamped dispersive KAW cascade ($-8/3$) and a cascade strongly suppressed by collisionless wave-particle interactions ($-11/3$) (Boldyrev and Perez, 2012; Passot and Sulem, 2015; Alexandrova et al., 2012), consistent with an intermediate dissipation state. The spectral index alone does not identify the specific dissipation channel, but it provides a straightforward

observational constraint that is accessible from burst-mode FGM data without particle measurements and that is well suited to multi-interval statistical surveys.

These results demonstrate that a combined multi-diagnostic electromagnetic approach, applied carefully to a high- β interval, provides a consistent and internally redundant identification of KAW activity, and that the kinetic-range spectral index from standard burst-mode magnetometer data carries direct information about the dissipation state of the turbulent cascade. The methodology is straightforward to apply to other MMS magnetosheath intervals and to future missions providing high-cadence burst-mode electromagnetic measurements.

Acknowledgments

MMS data are publicly available from the NASA Coordinated Data Analysis Web (CDAWeb) database at <https://cdaweb.gsfc.nasa.gov/>. Data analysis was performed using the PySPEDAS library (Angelopoulos et al., 2019; Grimes et al., 2022).

CRedit authorship contribution statement

Mani K Chettri: Conceptualization, Data curation, Software, Formal analysis, Writing – original draft. **Rupak Mukherjee:** Supervision, Writing – review & editing. **Hemam D. Singh:** Conceptualization, Supervision, Writing – review & editing.

References

- Afshari, A.S., Howes, G.G., Kletzing, C.A., Hartley, D.P., Boardsen, S.A., 2021. The importance of electron Landau damping for the dissipation of turbulent energy in terrestrial magnetosheath plasma. *Journal of Geophysical Research: Space Physics* 126, e2021JA029578. doi:10.1029/2021JA029578.
- Alexandrova, O., Lacombe, C., Mangeney, A., 2008. Spectra and anisotropy of magnetic fluctuations in the Earth's magnetosheath: Cluster observations. *Annales Geophysicae* 26, 3585–3596. doi:10.5194/angeo-26-3585-2008.
- Alexandrova, O., Lacombe, C., Mangeney, A., Grappin, R., Maksimovic, M., 2012. Solar wind turbulent spectrum at plasma kinetic scales. *The Astrophysical Journal* 760, 121. doi:10.1088/0004-637X/760/2/121.
- Angelopoulos, V., Cruce, P., Drozdov, A., Grimes, E.W., Hatzigeorgiou, N., King, D.A., Larson, D., Lewis, J.W., McTiernan, J.M., Roberts, D.A., Russell, C.L., Hori, T., Kasahara, Y., Kumamoto, A., Matsuoka, A., Miyashita, Y., Miyoshi, Y., Shinohara, I., Teramoto, M., Faden, J.B., Halford, A.J., McCarthy, M., Millan, R.M., Sample, J.G., Smith, D.M., Woodger, L.A., Masson, A., Narock, A.A., Asamura, K., Chang, T.F., Chiang, C.Y., Kazama, Y., Keika, K., Matsuda, S., Segawa, T., Seki, K., Shoji, M., Tam, S.W.Y., Umemura, N., Wang, B.J., Wang, S.Y., Redmon, R., Rodriguez, J.V., Singer, H.J., Vandegriff, J., Abe, S., Nose, M., Shinbori, A., Tanaka, Y.M., UeNo, S., Andersson, L., Dunn, P., Fowler, C., Halekas, J.S., Hara, T., Harada, Y., Lee, C.O., Lillis, R., Mitchell, D.L., Argall, M.R., Bromund, K., Burch, J.L., Cohen, I.J., Galloy, M., Giles, B., Jaynes, A.N., Le Contel, O., Oka, M., Phan, T.D., Walsh, B.M., Westlake, J., Wilder, F.D., Bale, S.D., Livi, R., Pulupa, M., Whittlesey, P., DeWolfe, A., Harter, B., Lucas, E., Auster, U., Bonnell, J.W., Cully, C.M., Donovan, E., Ergun, R.E., Frey, H.U., Jackel, B., Keiling, A., Korth, H., McFadden, J.P., Nishimura, Y., Plaschke, F., Robert, P., Turner, D.L., Weygand, J.M., Candey, R.M., Johnson, R.C., Kovalick, T., Liu, M.H., McGuire, R.E., Breneman, A., Kersten, K., Schroeder, P., 2019. The space physics environment data analysis system (spedas). *Space Science Reviews* 215, 9. doi:10.1007/s11214-018-0576-4.
- Bale, S.D., Kellogg, P.J., Mozer, F.S., Horbury, T.S., Rème, H., 2005. Measurement of the electric fluctuation spectrum of magnetohydrodynamic turbulence. *Physical Review Letters* 94, 215002. doi:10.1103/PhysRevLett.94.215002.
- Bandyopadhyay, R., Matthaeus, W.H., Parashar, T.N., Yang, Y., Chasapis, A., Giles, B.L., Gershman, D.J., Pollock, C.J., Russell, C.T., Strangeway, R.J., Torbert, R.B., Moore, T.E., Burch, J.L., 2020. Statistics of kinetic dissipation in the Earth's magnetosheath: MMS observations. *Physical Review Letters* 124, 255101. doi:10.1103/PhysRevLett.124.255101.
- Boldyrev, S., Perez, J.C., 2012. Spectrum of kinetic-alfvén turbulence. *The Astrophysical Journal Letters* 758, L44. doi:10.1088/2041-8205/758/2/L44.
- Burch, J.L., Moore, T.E., Torbert, R.B., Giles, B.L., 2016. MMS overview and science objectives. *Space Science Reviews* 199, 5–21. doi:10.1007/s11214-015-0164-9.
- Chen, C.H.K., Klein, K.G., Howes, G.G., 2019. Evidence for electron Landau damping in space plasma turbulence. *Nature Communications* 10, 740. doi:10.1038/s41467-019-08435-3.
- Chettri, M.K., Shrivastav, V., Mukherjee, R., Gaur, N., Sharma, R., Singh, H.D., 2024. Nonlinear coupling of kinetic alfvén waves and ion acoustic waves in the inner heliosphere. *Research in Astronomy and Astrophysics* 24, 105009.
- Chettri, M.K., Singh, H.D., Mukherjee, R., 2026. Mms observations of kinetic alfvén wave turbulence and steep kinetic-range spectra in the outer plasma sheet boundary layer. *arXiv preprint arXiv:2603.07969*.
- Chettri, M.K., Singh, H.D., Shrivastav, V., Singh, B., Mukherjee, R., 2025. Damped kinetic alfvén waves in earth's magnetosheath: Numerical simulations and mms observations. *arXiv preprint arXiv:2512.09828*.
- Ergun, R.E., Tucker, S., Westfall, J., Goodrich, K.A., Malaspina, D.M., Summers, D., Wallace, J., Karlsson, M., Mack, J., Brennan, N., Pyke, B., Withnell, P., Torbert, R., Macri, J., Rau, D., Dors, I., Needell, J., Lindqvist, P.A., Olsson, G., Cully, C.M., 2016. The axial double probe and fields signal processing for the MMS mission. *Space Science Reviews* 199, 167–188. doi:10.1007/s11214-014-0115-x.

- Gershman, D.J., F-Viñas, A., Dorelli, J.C., Boardsen, S.A., Avanos, L.A., Bellan, P.M., Schwartz, S.J., Lavraud, B., Coffey, V.N., Chandler, M.O., Saito, Y., Paterson, W.R., Fuselier, S.A., Ergun, R.E., Strangeway, R.J., Russell, C.T., Giles, B.L., Pollock, C.J., Torbert, R.B., Burch, J.L., 2017. Wave-particle energy exchange directly observed in a kinetic alfvén wave. *Nature Communications* 8, 14719. doi:10.1038/ncomms14719.
- Grimes, E.W., Harter, B., Hatzigeorgiu, N., Drozdov, A., Lewis, J.W., Angelopoulos, V., Cao, X., Chu, X., Hori, T., Matsuda, S., Jun, C.W., Nakamura, S., Kitahara, M., Segawa, T., Miyoshi, Y., Le Contel, O., 2022. The spedas framework. *Frontiers in Astronomy and Space Sciences* 9, 1020815. doi:10.3389/fspas.2022.1020815.
- Hadid, L.Z., Sahraoui, F., Galtier, S., 2017. Energy cascade rate in compressible fast and slow solar wind turbulence. *The Astrophysical Journal* 838, 9. doi:10.3847/1538-4357/aa603f.
- Hadid, L.Z., Sahraoui, F., Galtier, S., Huang, S.Y., 2018. Compressible magnetohydrodynamic turbulence in the Earth's magnetosheath: Estimation of the energy cascade rate using in situ spacecraft data. *Physical Review Letters* 120, 055102. doi:10.1103/PhysRevLett.120.055102.
- Hasegawa, A., 1976. Particle acceleration by MHD surface wave and formation of aurora. *Journal of Geophysical Research* 81, 5083–5090. doi:10.1029/JA081i028p05083.
- Hollweg, J.V., 1999. Kinetic alfvén wave revisited. *Journal of Geophysical Research: Space Physics* 104, 14811–14819. doi:10.1029/1998JA900132.
- Horvath, S.A., Howes, G.G., McCubbin, A.J., 2020. Electron Landau damping of kinetic Alfvén waves in simulated magnetosheath turbulence. *Physics of Plasmas* 27, 102901. doi:10.1063/5.0021727.
- Howes, G.G., 2015. Kinetic turbulence, in: Lazarian, A., de Gouveia Dal Pino, E.M., Melioli, C. (Eds.), *Magnetic Fields in Diffuse Media*. Springer, Berlin, Heidelberg, pp. 123–152. doi:10.1007/978-3-662-44625-6_6.
- Howes, G.G., Dorland, W., Cowley, S.C., Hammett, G.W., Quataert, E., Schekochihin, A.A., Tatsuno, T., 2008. Kinetic simulations of magnetized turbulence in astrophysical plasmas. *Physical Review Letters* 100, 065004. doi:10.1103/PhysRevLett.100.065004.
- Howes, G.G., Klein, K.G., TenBarge, J.M., 2014. Validity of the Taylor hypothesis for linear kinetic waves in the weakly collisional solar wind. *The Astrophysical Journal* 789, 106. doi:10.1088/0004-637X/789/2/106.
- Klein, K.G., Howes, G.G., TenBarge, J.M., 2014. The violation of the Taylor hypothesis in measurements of solar wind turbulence. *The Astrophysical Journal Letters* 790, L20. doi:10.1088/2041-8205/790/2/L20.
- Leamon, R.J., Smith, C.W., Ness, N.F., Matthaeus, W.H., Wong, H.K., 1998. Observational constraints on the dynamics of the interplanetary magnetic field dissipation range. *Journal of Geophysical Research: Space Physics* 103, 4775–4787. doi:10.1029/97JA03394.
- Lucek, E.A., Constantinescu, D., Goldstein, M.L., Pickett, J., Pinçon, J.L., Sahraoui, F., Treumann, R.A., Walker, S.N., 2005. The magnetosheath. *Space Science Reviews* 118, 95–152. doi:10.1007/s11214-005-3825-2.
- Lysak, R.L., Lotko, W., 1996. On the kinetic dispersion relation for shear alfvén waves. *Journal of Geophysical Research: Space Physics* 101, 5085–5094. doi:10.1029/95JA03712.
- Macek, W.M., Krasnińska, A., Silveira, M.V.D., Sibeck, D.G., Wawrzaszek, A., Burch, J.L., Russell, C.T., 2018. Intermittent turbulence in the Magnetospheric Multiscale mission data. *The Astrophysical Journal Letters* 864, L29. doi:10.3847/2041-8213/aad9a8.
- Macek, W.M., Wójcik, D., 2023. Intermittency and multifractality in magnetosheath turbulence. *Monthly Notices of the Royal Astronomical Society* 526, 5779–5790. doi:10.1093/mnras/stad2584.
- Passot, T., Sulem, P.L., 2015. A model for the non-universal power law of the solar wind sub-ion-scale magnetic spectrum. *The Astrophysical Journal Letters* 812, L37. doi:10.1088/2041-8205/812/2/L37.
- Pollock, C., Moore, T., Jacques, A., Burch, J., Gliese, U., Saito, Y., Omoto, T., Avanos, L., Barrie, A., Coffey, V., Dorelli, J., Gershman, D., Giles, B., Rosnack, T., Salo, C., Yokota, S., Adrian, M., Aoustin, C., Auletta, C., Aung, S., Bigio, V., Cao, N., Chandler, M., Chornay, D., Christian, K., Clark, G., Collinson, G., Corris, T., De Los Santos, A., Devlin, R., Diaz, T., Dickerson, T., Dickson, C., Diekmann, A., Diggs, F., Duncan, C., Figueroa-Vinas, A., Firman, C., Freeman, M., Galassi, N., Garcia, K., Goodhart, G., Guerrerro, D., Hageman, J., Hanley, J., Hemminger, E., Holland, M., Hutchins, M., James, T., Jones, W., Kreisler, S., Kujawski, J., Lavu, V., Lobell, J., LeCompte, E., Lukemire, A., MacDonald, E., Mariano, A., Mukai, T., Narayanan, K., Nguyen, Q., Onizuka, M., Paterson, W., Persyn, S., Piepgrass, B., Cheney, F., Rager, A., Raghuram, T., Ramil, A., Reichenthal, L., Rodriguez, H., Rouzaud, J., Rucker, A., Saito, Y., Samara, M., Sauvaud, J.A., Schuster, D., Shappirio, M., Shelton, K., Sher, D., Smith, D., Smith, K., Smith, S., Steinfeld, D., Szymkiewicz, R., Tanimoto, K., Taylor, J., Tucker, C., Tull, K., Uhl, A., Vloet, J., Walpole, P., Weidner, S., White, D., Winkert, G., Yeh, P.S., Zeuch, M., 2016. Fast plasma investigation for Magnetospheric Multiscale. *Space Science Reviews* 199, 331–406. doi:10.1007/s11214-016-0245-4.
- Roberts, O.W., Toledo-Redondo, S., Perrone, D., Zhao, J., Narita, Y., Gershman, D., Nakamura, R., Lavraud, B., Escoubet, C.P., Giles, B., Dorelli, J., Pollock, C., Burch, J., 2018. Ion-scale kinetic alfvén turbulence: MMS observations of the alfvén ion cyclotron instability and inhomogeneous heating. *Geophysical Research Letters* 45, 7974–7983. doi:10.1029/2018GL078498.
- Russell, C.T., Anderson, B.J., Baumjohann, W., Bromund, K.R., Dearborn, D., Fischer, D., Le, G., Leinweber, H.K., Leneman, D., Magnes, W., Means, J.D., Moldwin, M.B., Nakamura, R., Pierce, D., Plaschke, F., Rowe, K.M., Slavin, J.A., Strangeway, R.J., Torbert, R., Hagen, C., Jernej, I., Valavanoglou, A., Richter, I., 2016. The Magnetospheric Multiscale magnetometers. *Space Science Reviews* 199, 189–256. doi:10.1007/s11214-014-0057-3.
- Sahraoui, F., Goldstein, M.L., Belmont, G., Canu, P., Rezeau, L., 2010. Three-dimensional anisotropic k spectra of turbulence at subproton scales in the solar wind. *Physical Review Letters* 105, 131101. doi:10.1103/PhysRevLett.105.131101.
- Sahraoui, F., Goldstein, M.L., Robert, P., Khotyaintsev, Y.V., 2009. Evidence of a cascade and dissipation of solar-wind turbulence at the electron gyroscale. *Physical Review Letters* 102, 231102. doi:10.1103/PhysRevLett.102.231102.
- Sahraoui, F., Hadid, L., Huang, S., 2020. Magnetohydrodynamic and kinetic scale turbulence in the near-Earth space plasmas: A (short) biased review. *Reviews of Modern Plasma Physics* 4, 4. doi:10.1007/s41614-020-0040-2.
- Salem, C.S., Howes, G.G., Sundkvist, D., Bale, S.D., Chaston, C.C., Chen, C.H.K., Mozer, F.S., 2012. Identification of kinetic Alfvén wave turbulence in the solar wind. *The Astrophysical Journal Letters* 745, L9. doi:10.1088/2041-8205/745/1/L9.
- Schekochihin, A.A., Cowley, S.C., Dorland, W., Hammett, G.W., Howes, G.G., Quataert, E., Tatsuno, T., 2009. Astrophysical gyrokinetics: Kinetic and fluid turbulent cascades in magnetized weakly collisional plasmas. *The Astrophysical Journal Supplement Series* 182, 310–377.

doi:10.1088/0067-0049/182/1/310.

- Stasiewicz, K., Bellan, P., Chaston, C., Kletzing, C., Lysak, R., Maggs, J., Pokhotelov, O., Seyler, C., Shukla, P., Stenflo, L., Streltsov, A., Wahlund, J.E., 2000. Small scale Alfvénic structures in the aurora. *Space Science Reviews* 92, 423–533. doi:10.1023/A:1005207202143.
- Stawarz, J.E., Eastwood, J.P., Phan, T.D., Gingell, I.L., Pyakurel, P.S., Shay, M.A., Robertson, S.L., Russell, C.T., Le Contel, O., 2022. Turbulence-driven magnetic reconnection in a low-beta magnetosheath. *Physics of Plasmas* 29, 012901. doi:10.1063/5.0071106.
- Stawarz, J.E., Genestreti, K.J., 2023. Observations of coherent structures and turbulence in the magnetosheath. *Physics of Plasmas* 30, 120401. doi:10.1063/5.0171488.
- Taylor, G.I., 1938. The spectrum of turbulence. *Proceedings of the Royal Society of London. Series A, Mathematical and Physical Sciences* 164, 476–490. doi:10.1098/rspa.1938.0032.
- TenBarge, J.M., Howes, G.G., 2013. Current sheets and collisionless damping in kinetic plasma turbulence. *The Astrophysical Journal Letters* 771, L27. doi:10.1088/2041-8205/771/2/L27.
- Torbert, R.B., Russell, C.T., Magnes, W., Ergun, R.E., Lindqvist, P.A., LeContel, O., Vaith, H., Macri, J., Myers, S., Rau, D., Needell, J., King, B., Granoff, M., Chutter, M., Dors, I., Olsson, G., Khotyaintsev, Y.V., Eriksson, A., Kletzing, C.A., Bounds, S., Anderson, B., Baumjohann, W., Steller, M., Bromund, K., Le, G., Nakamura, R., Strangeway, R.J., Leinweber, H.K., Tucker, S., Westfall, J., Fischer, D., Plaschke, F., Porter, J., Lappalainen, K., 2016. The FIELDS instrument suite on MMS: Scientific objectives, measurements, and data products. *Space Science Reviews* 199, 105–135. doi:10.1007/s11214-014-0109-8.
- Welch, P.D., 1967. The use of fast Fourier transform for the estimation of power spectra. *IEEE Transactions on Audio and Electroacoustics* 15, 70–73. doi:10.1109/TAU.1967.1161901.
- Wygant, J.R., Keiling, A., Cattell, C.A., Lysak, R.L., Temerin, M., Mozer, F.S., Kletzing, C.A., Scudder, J.D., Streltsov, V., Lotko, W., Russell, C.T., 2002. Evidence for kinetic alfvén waves and parallel electron energization at 4–6 R_E altitudes. *Journal of Geophysical Research: Space Physics* 107, SMP 24–1–SMP 24–13. doi:10.1029/2001JA900113.

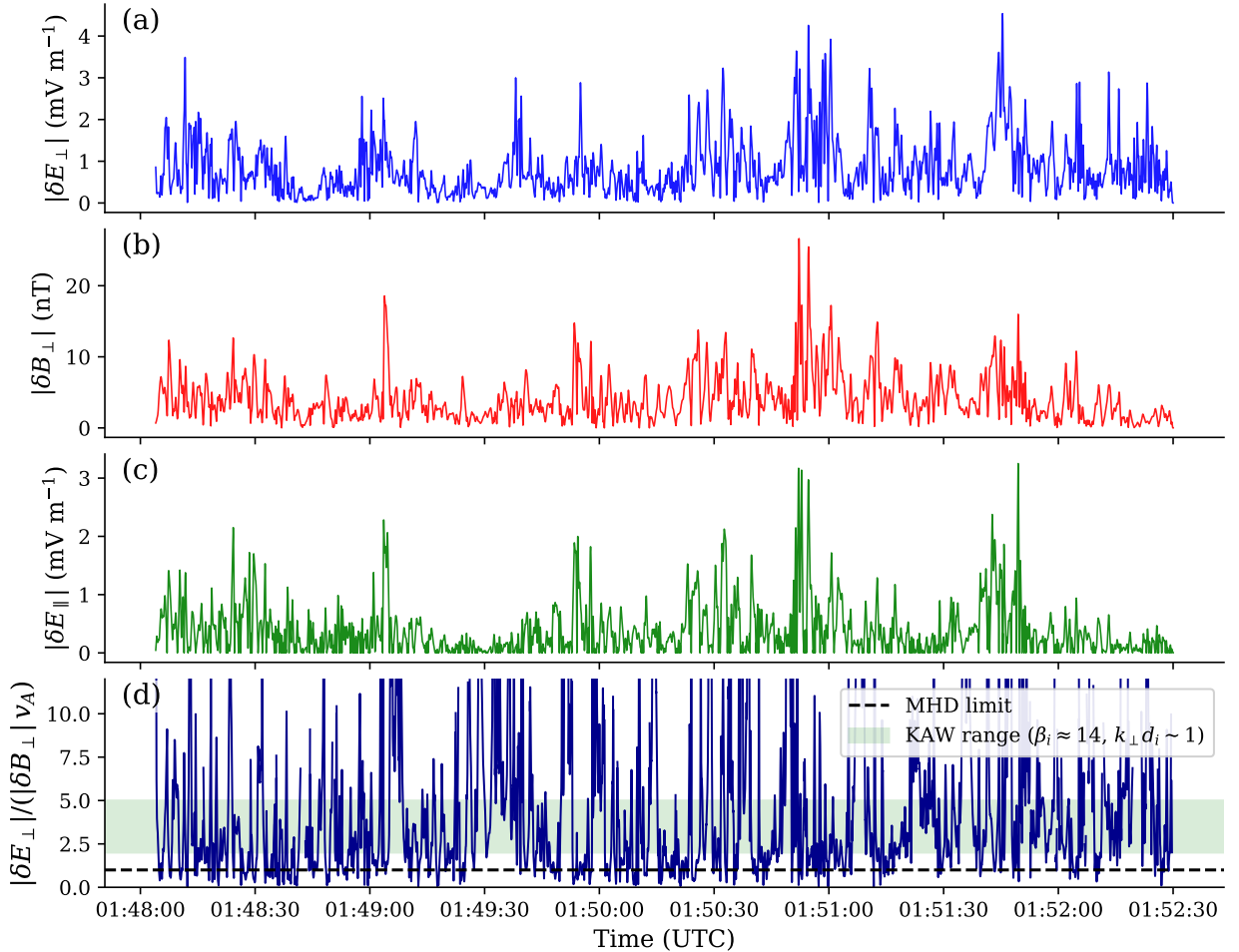


Figure 1: MMS1 electromagnetic field analysis, 2015 December 28, 01:48:00–01:52:30 UT ($\beta_i = 14.4$, $V_{\text{flow}} = 159 \text{ km s}^{-1}$). (a) Amplitude of perpendicular electric field fluctuations δE_{\perp} (RMS 1.08 mV m^{-1} , peak 4.5 mV m^{-1}). (b) Amplitude of perpendicular magnetic field fluctuations δB_{\perp} (RMS 5.22 nT , peak $\sim 27 \text{ nT}$). (c) Amplitude of parallel electric field δE_{\parallel} (peak 3.2 mV m^{-1}). (d) Normalized ratio $\delta E_{\perp}/(\delta B_{\perp}v_A)$ (median 2.55 , IQR 1.43 – 5.00). The black dashed line marks the ideal MHD limit (ratio = 1); the green shaded region indicates the expected range for KAWs at $\beta_i \approx 14$. A $[0.1, 2.0]$ Hz bandpass and 10 s background subtraction are applied.

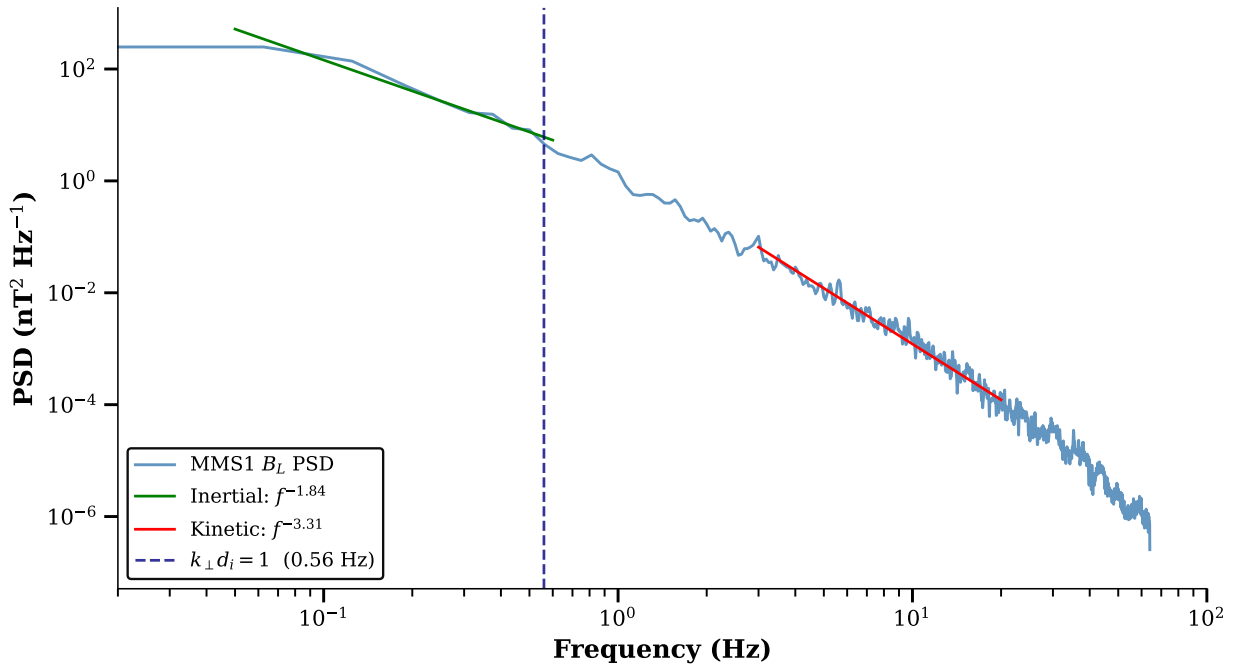


Figure 2: Magnetic power spectral density of the B_L component (LMN coordinates) from MMS1 burst-mode FGM data, Welch method ($N_{\text{seg}} = 2048$, Hanning window, 50% overlap). Green line: inertial-range power-law fit $f^{-1.84}$ (0.05–0.6 Hz), steepened relative to the Kolmogorov slope by the compressibility and shock-processing of the magnetosheath. Red line: kinetic-range fit $f^{-3.31}$ (3–20 Hz). The bright green vertical line marks $k_{\perp} d_i = 1$ at 0.56 Hz, confirming that the spectral break near 0.6 Hz corresponds to the ion inertial scale for the measured bulk flow $V_{\text{flow}} = 159 \text{ km s}^{-1}$. The kinetic index -3.31 lies between the theoretical limits $-8/3$ (Boldyrev and Perez, 2012) and $-11/3$ (Passot and Sulem, 2015; Alexandrova et al., 2012), consistent with an intermediate wave-particle interaction state.

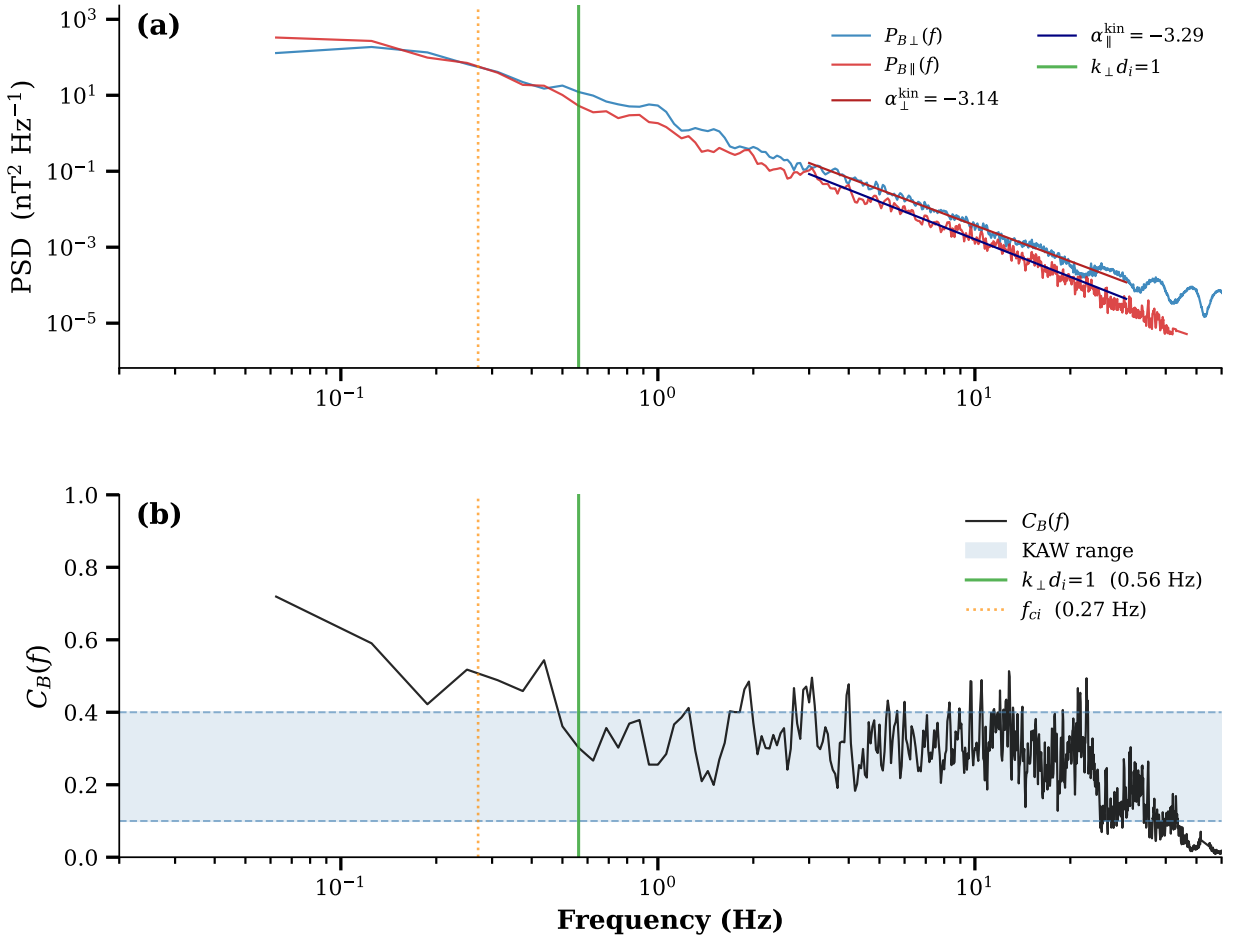


Figure 3: Magnetic polarization and compressibility from MMS1 burst-mode FGM data decomposed in field-aligned coordinates (FAC). (a) Perpendicular ($P_{B\perp}$, blue) and parallel ($P_{B\parallel}$, red) magnetic power spectra, with kinetic-range power-law fits ($\alpha_{\perp}^{\text{kin}} = -3.14$ in firebrick, $\alpha_{\parallel}^{\text{kin}} = -3.29$ in navy) overplotted above the ion-scale break. The inertial-range scaling is reported in Figure 2. (b) Magnetic compressibility $C_B(f) = P_{B\parallel}/(P_{B\parallel} + P_{B\perp})$; the blue-shaded band marks the theoretical KAW range $C_B \in [0.10, 0.40]$ (Sahraoui et al., 2009; Stasiewicz et al., 2000), with the upper bound explicitly marked by a horizontal dashed line for visual reference. In both panels the green vertical line marks $k_{\perp} d_i = 1$ (0.56 Hz) and the orange dotted line marks $f_{ci} = 0.27$ Hz. Above the ion-scale break, $P_{B\perp}/P_{B\parallel} \approx 2.2$ (transverse-dominated fluctuations) and $C_B \approx 0.31$ (median), consistent with KAWs and inconsistent with mirror modes ($C_B \sim 0.8-1.0$) or whistler-mode waves ($C_B \gtrsim 0.5$).